communications earth & environment

Article

A Nature Portfolio journal

https://doi.org/10.1038/s43247-025-03059-6

Declining number of northern hemisphere land-surface frozen days under global warming and thinner snowpacks

Shadi Hatami [1,2], Masoud Zaerpour [1] ✉, André S. Ballarin[3], Jan Franklin Adamowski[2,4], Simon Michael Papalexiou [1,5,6], Alain Pietroniro[1] & John S. Kimball[7]

Freeze–thaw processes shape ecosystems, hydrology, and infrastructure across northern high latitudes. Here we use satellite-based observations from 1979–2021 across 47 northern hemisphere ecoregions to examine changes in the number of frozen land-surface days per year. We find widespread declines, with 70% of ecoregions showing significant reductions, primarily linked to rising air temperatures and thinning snowpacks. Causal analysis demonstrates that air temperature and snow depth exert consistent controls on the number of frozen days. A trend-informed assessment based on historical observations suggests a potential average loss of more than 30 frozen days per year by the end of the century, with the steepest decreases in Alaska, northern Canada, northern Europe, and eastern Russia. Scenario-based analysis indicates that each 1 °C increase in air temperature reduces frozen days by ~6-days, while each 1 cm decrease in snow depth leads to a ~ 3-day reduction. These shifts carry major ecological and socio-economic implications.

In a typical year, over one-third of the land across the globe undergoes an abrupt near 0 °C seasonal transition between predominantly frozen and non-frozen (thawed) conditions[1]. Freeze-thaw (FT) dynamics refer to these transitions of the land surface – including the upper soil layer, vegetation, and any snow cover – typically associated with seasonal temperature fluctuations, which can vary in frequency and timing across regions. FT processes are among the defining land-surface characteristics in higher latitudes. The regional dynamics of FT can physically affect hydrological[2], climatic[3], geological[4], and ecological[5] processes, as well as impact socio-economic activities such as agricultural productivity, infrastructure stability, and the cultural and economic livelihoods of northern communities[6]. FT dynamics alter the soil density, hydraulic conductivity, and infiltration[7–11], which can impact both surface and sub-surface connectivity and the water, carbon, and other matter pathways throughout the soil[12–17]. FT dynamics affect the energy and water balance[18,19] and land-atmospheric interactions[20], controlling vegetation growth and wildlife, and potentially agriculture and resource development[21–23]. In this study, we focus on one key manifestation of FT processes – Number of Frozen Days (NF). NF is defined as the total number of days per year when the land surface is in a frozen state in both morning (AM) and afternoon (PM) measurements of a given day. While NF does not capture individual FT events, it serves as a proxy for cumulative exposure to frozen conditions, which holds ecological and infrastructural relevance. It is important to note that NF captures only the duration of surface frozen conditions and does not directly reflect other dimensions of freeze–thaw dynamics, such as the depth and intensity of soil freezing or the frequency of within-season freeze–thaw events. Accordingly, NF should be interpreted as a measure of the satellite-observed surface state rather than subsurface or permafrost freezing.

The FT influence is generally greater in higher latitude northern hemisphere ecoregions where the potential growing season is constrained by an extended annual frozen period[24]. However, the FT dynamics may be changing as a consequence of global warming, with potential impacts on soil structure, hydrological regulation, and carbon cycling that underpin key ecosystem services[25]. The rate of FT changes may also be more intense in the high northern latitudes due to the polar amplification of global warming[26] and the presence of extensive permafrost, which is becoming increasingly vulnerable to thaw with warmer temperatures and a shorter frozen season[27–29]. Hence, it is essential to clarify FT trends and driving factors to better inform decision-making and mitigate potential negative impacts on regional ecosystems and human development.

[1]Department of Civil Engineering, Schulich School of Engineering, University of Calgary, Calgary, AL, Canada. [2]Department of Bioresource Engineering, McGill University, Montreal, QC, Canada. [3]Department of Hydraulics and Sanitation, São Carlos School of Engineering, University of São Paulo, São Paulo, Brazil. [4]United Nations University Institute for Water, Environment and Health (UNU-INWEH), Richmond Hill, ON, Canada. [5]Institute of Global Water Security, Hamburg University of Technology, Hamburg, Germany. [6]Institute for Water, Environment and Health, United Nations University, Hamilton, ON, Canada. [7]Numerical Terradynamic Simulation Group, W.A. Franke College of Forestry and Conservation, University of Montana, Missoula, MT, USA. ✉e-mail: masoud.zaerpour@ucalgary.ca

Although local factors like vegetation, soil organic matter, solar radiation, and wildfires can influence FT dynamics[30–32], at the regional and continental scale, surface air temperature and snow depth emerge as the most dominant drivers[33–37]. Hence, a warming climate can profoundly impact soil temperature patterns and the dynamics of FT. Air temperature is widely used in FT studies as a practical and physically meaningful proxy for surface energy balance, especially over large spatial and temporal scales. This follows the logic of degree-day approaches commonly applied to snow and ice melt modeling, where air temperature serves as an integrative indicator of net radiative and turbulent energy fluxes influencing the frozen state of the landscape. Rising air temperatures can affect the timing and duration of FT cycles by shortening the frozen season, deepening the active soil layer, extending the length of the thaw-period, while leading to permafrost retreat[38,39]. Simultaneously, reduced snow depth limits the insulation of the ground surface, making near-surface conditions more directly responsive to air temperature fluctuations. This increases exposure and vulnerability to extreme events[40,41] while changing the surface albedo and subsequent energy balance[42–44]. In addition to the quantity of snow, its quality, including albedo, density, and layering, strongly influences the surface energy balance by controlling both reflectivity and insulation. These factors contribute to the well-documented non-linear amplification of warming, where small changes in snow depth and ice cover can produce disproportionately large climate responses[45,46].

It has been well documented that climate change has both greatly impacted air temperature and snow depth and thus FT dynamics in both time and space[3,47–49]. These alterations can shift the timing and the length of the freezing period, the thickness of the frozen layer, and the frequency of transitions between frozen and thawed states[50,51]. Currently, approximately one-third of the Earth's land area undergoes seasonal transitions in FT dynamics, and these transitions are projected to occur more frequently and to shift in timing in response to future climate change[52]. Regionally, variations exist, with more pronounced changes in FT cycles observed at northern latitudes attributed to the accelerated pace of warming temperatures in those areas[53]. FT dynamics are commonly monitored using satellite-based passive microwave observations, which provide consistent long-term records and global coverage across high latitudes. In this study, we use such a dataset derived from calibrated radiometric brightness temperatures captured between 1979 and 2021 from four satellite-based passive microwave sensors: the Scanning Multichannel Microwave Radiometer (SMMR), the Special Sensor Microwave/Imager (SSM/I), the Special Sensor Microwave Imager/Sounder (SSMIS), and the Advanced Microwave Scanning Radiometer 2 (AMSR2)[54]. The changes in FT dynamics can cause shifts in regional phenology, net ecosystem productivity, and other biogeochemical processes, with some triggering feedback effects, such as increased greenhouse gas emissions from thawing landscapes, exacerbating global warming[55–57]. The changing FT cycles can further promote permafrost thaw and soil erosion, impacting human infrastructure, landscape hydrology, and water quality[58,59]. Hence, understanding potential changes in FT dynamics under future climate conditions is crucial for addressing their diverse socio-economic and environmental consequences and developing adaptive strategies[14,60,61].

Such considerations drive our interest to characterize the effects of warming temperature and changing snow depth on FT processes across the global northern hemisphere high latitude (≥45 °N) ecoregions. For this purpose, we used surface meteorological reanalysis data from the European Centre for Medium-Range Weather Forecasts - ReAnalysis 5 (ERA5)[62], and the satellite observation-based global landscape FT Earth System Data Record (FT-ESDR) from the National Snow and Ice Data Center archive (https://nsidc.org/data/nsidc-0477/versions/5)[63]. ERA5 provides a consistent, comprehensive surface meteorology data record that includes detailed snow properties derived from an advanced Earth system model and an observational data assimilation system. The FT-ESDR provides a complementary satellite observational record of land surface FT conditions derived from passive microwave radiometry. The FT-ESDR documents changes in the predominant frozen or non-frozen condition of the land surface under nearly all weather conditions, providing a near-continuous long-term daily freeze-thaw record to assess FT trends and connections to relevant climate variables over the northern hemisphere[53]. Despite increasing attention to FT dynamics, few studies have explicitly examined the compound influence of warming temperatures and thinning snowpacks on the annual number of frozen days (NF) at a large scale, particularly through a causal inference lens. NF serves as an integrated indicator of how frequently landscapes experience freezing conditions within a given FT year (defined from Sep 1 to Aug 31), with implications for vegetation phenology, soil processes, carbon fluxes, and infrastructure stability. By focusing on NF, our study captures the frequency of frozen ground conditions across the FT year, providing insight into how often landscapes experience freezing under changing climate conditions. While NF does not explicitly represent the persistence or duration of individual freeze periods, it serves as an important proxy for assessing cumulative freezing exposure across northern regions. Furthermore, by quantifying both the trends and causal drivers of NF across 47 northern ecoregions, this work provides insights into how climatic forcing mechanisms shape FT functioning in a warming world. The causal discovery algorithm employed systematically identifies directional dependencies in time series data, making it well-suited for analyzing the complex interactions between climatic factors and NF. This investigation centers on changes in the number of days with the frozen state in each year, referred to as NF hereafter, which represents the total frozen-day count as a proxy for the broader FT regime. While the FT-ESDR enables detection of daily FT transitions, we focus specifically on the estimated total number of frozen days (NF) due to its broader ecological and operational implications, including impacts on phenological, hydrological, and agricultural processes, natural resource accessibility, and the stability of infrastructure in cold regions[64–66]. We employ causal discovery in parallel to the copula conditional multivariate framework[67–69] to address three main research questions: (1) How are the NF changing over recent decades? (2) What are the leading causes of these changes? (3) How will different levels of change in surface air temperature and snow depth impact NF across the northern hemisphere into the near future? This study advances earlier work (e.g., Hatami & Nazemi[33]) by scaling up to 47 northern-hemisphere ecoregions, introducing an integrated causal discovery–copula framework that combines causal inference with probabilistic modeling, and enhancing the forward-looking analysis with systematically defined scenarios and a trend-informed extrapolation. These innovations provide a geographically comprehensive and methodologically distinct assessment of frozen-day dynamics.

Results and discussion

To assess how FT dynamics have evolved over recent decades, we analyzed spatial and temporal variations in the number of frozen days (NF), air temperature, and snow depth across 47 ecoregions in the northern hemisphere from 1979 to 2021. This analysis establishes a baseline for understanding the broader changes in NF before investigating their causal relationships and future projections.

We first examined the long-term average and trends in the variables under consideration, namely, the annual count of frozen days (NF), air temperature, and snow depth, spanning the observed period (1979-2021). Specifically, we investigated the long-term average values (Fig. 1a–c) as well as the potential trends in the mentioned variables (Fig. 1d–f) over the observed period in each ecoregion.

Our findings reveal substantial spatial variability in air temperature trends across the study area. Long-term average annual air temperatures range from approximately −13 °C to +12 °C across different ecoregions, with an overall mean of 0 °C. Notably, nearly 85% of the ecoregions experience significantly increasing temperature trends, while in the remaining 15%, the annual average air temperature increase is not significant ($p < 0.05$). The rate of warming air temperature, where trends are significant, is generally higher for ecozones located in higher latitudes, consistent with the well-documented pattern of amplified warming in northern regions[70]. The long-term average snow depth over the studied ecoregions ranges from 0.5 cm to above 25 cm, with an average of 15 cm.

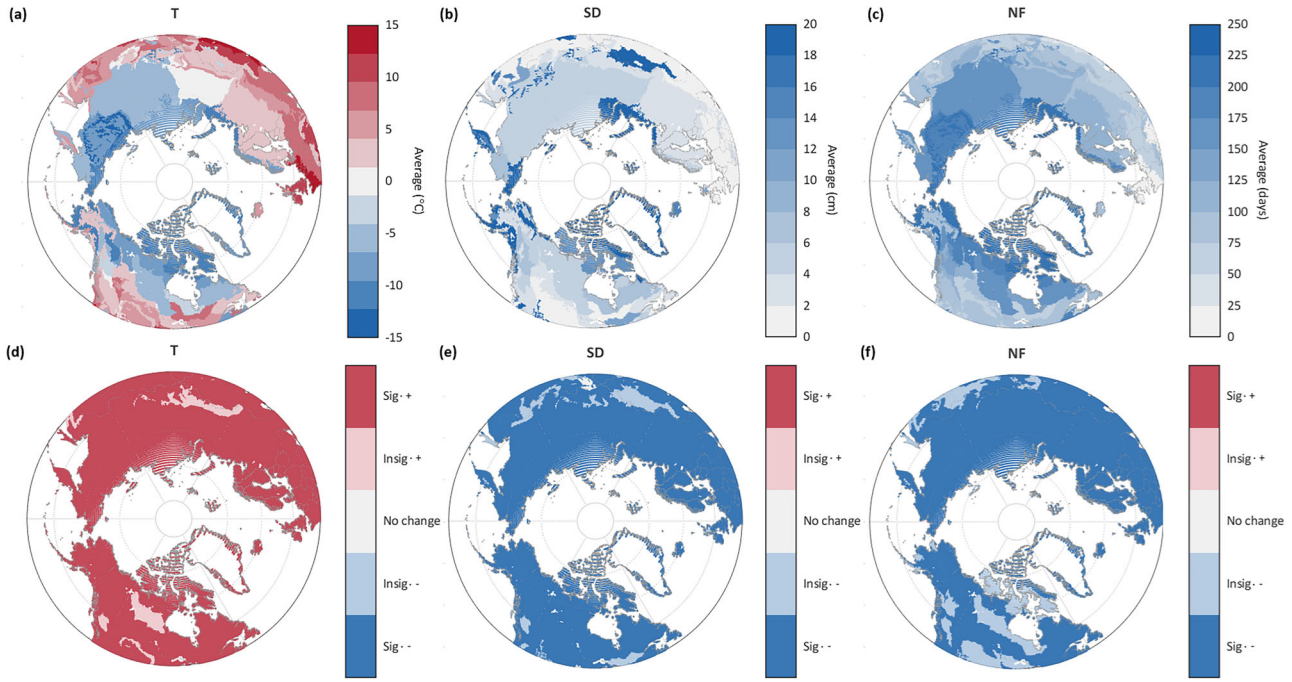

Fig. 1 | Long-term average and trends of air temperature, snow depth, and number of frozen days (NF) across northern ecoregions (≥45° N) from 1979–2021. a–c show the long-term mean annual air temperature, snow depth, and NF, while **d–f** display the corresponding temporal trends for each ecoregion. Red and blue color codes show the respective positive and negative long-term averages or trends. White color denotes masked grid cells (e.g., open water and glacierized or sea-ice covered regions), and gray color shows areas with no significant trends indicated.

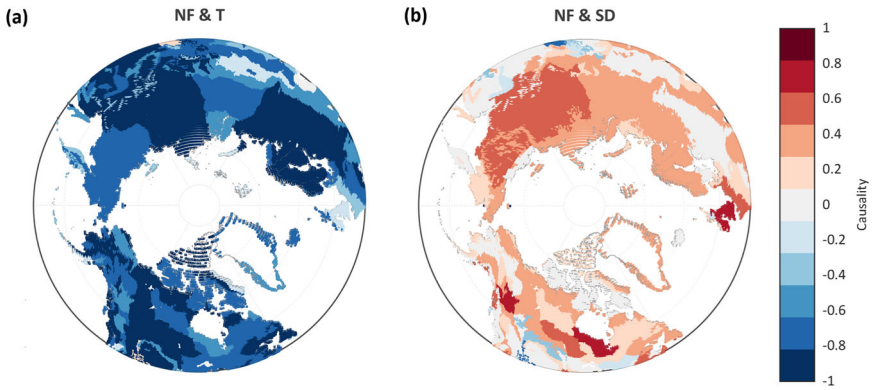

Fig. 2 | Causal relationships between the number of frozen days (NF) and its climatic drivers across northern ecoregions. a and **b** show the statistically inferred causal links between NF and air temperature, and between NF and snow depth, respectively. The blue and red color codes represent the negative and positive causal relationships, respectively.

Over 85% of the ecoregions exhibit significant decreasing trends in annual average snow depth, 13% show insignificant decreases, and 2% display no considerable changes. The observed snow depth reductions are consistent with studies finding thinner snowpacks due to warmer climates[71]. While we use annual average snow depth as a tractable, large-scale indicator in this study, we note that more commonly reported snow metrics include annual maximum depth, cumulative snowfall, or snow-cover duration. Nevertheless, annual average depth has been employed as a meaningful proxy in large-scale cryosphere studies, as it integrates information about both snow accumulation and persistence (e.g., ref. 33,71–75). Including this metric allows for consistent comparisons across ecoregions and years, and provides an interpretable signal of broad-scale snowpack trends, even if it does not fully capture the range of snow dynamics observable at daily scales. Finally, the long-term average NF exhibits a wide span, fluctuating from 30 to 250 days, with an average of 120 days. Nonetheless, the trend analysis indicates a significant decrease in NF in more than 70% of the ecoregions, whereas the remaining 30% exhibit statistically insignificant decreasing trends. These findings emphasize the imperative of addressing the changes in FT dynamics under a warming climate. NF spatial and temporal patterns represent the patterns of satellite-observed surface freeze–thaw state and should not be interpreted as subsurface soil or permafrost freezing. While surface and shallow soil temperatures often align in cold, snow-sparse regions, thick or persistent snowpacks can insulate the soil and decouple it from surface freeze signals. Therefore, NF is best viewed as an indicator of cumulative surface frozen exposure rather than of soil freeze depth or event frequency.

We also investigate the influence of air temperature and snow depth on NF using the PCMCI+ causal discovery algorithm, which is a statistical framework designed to infer directed dependencies based on temporal ordering and conditional independence tests – see Fig. 2. The PCMCI+ framework enables the identification of statistically directed relationships rather than simple correlations, distinguishing direct effects from indirect or mediated ones. While we acknowledge the seasonality of FT cycles, we use annual aggregates to ensure comparability between variables and across years. Annual aggregation helps smooth out fluctuations and regional differences in seasonal timing, making it possible to systematically assess long-

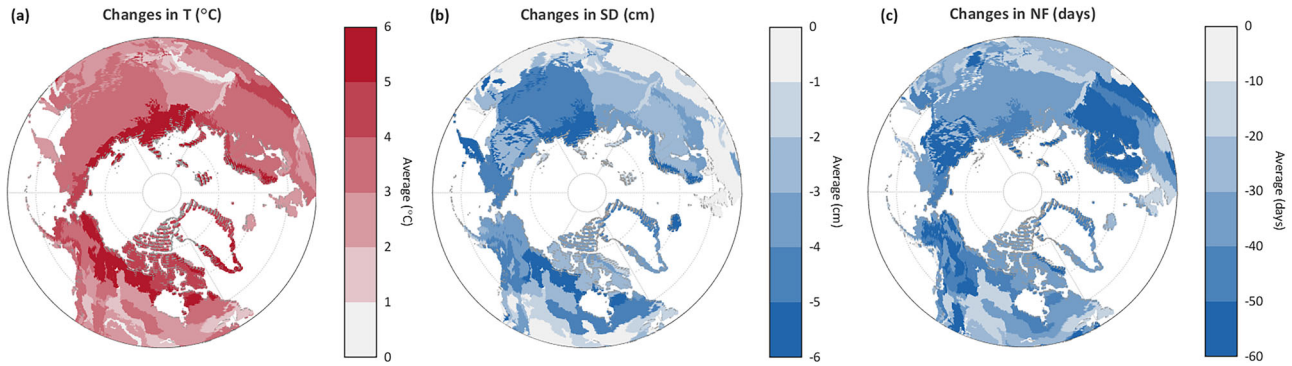

Fig. 3 | Projected future changes in air temperature, snow depth, and number of frozen days (NF) across northern ecoregions by the end of the century. a and **b** show projected changes in annual mean air temperature (T, °C) and snow depth (SD, cm) derived from the "linear extrapolation", while **c** illustrates the corresponding projected change in NF (days). The red and blue colors show increasing and decreasing changes, respectively.

term trends and interdependencies in a consistent way. This is particularly important when applying multivariate statistical and causal discovery methods, which benefit from uniform temporal granularity across variables. Similar frameworks have been effectively applied in previous studies to assess climate impacts on FT dynamics and cold-region processes[33,76]. Looking at the causal link between the annual air temperature and NF (Fig. 2a), there are significant causal strengths between the mentioned variables in almost all ecoregions of the northern hemisphere. The causal effect strength ranges from −0.1 to −0.9, with an average of −0.7 across all ecoregions. Considering the causal link between the annual snow depth and NF (Fig. 2b), we observe greater variability in the results among ecoregions. As noted above, NF reflects the satellite-observed surface freeze–thaw state, while snow depth is used here as a driver variable. The causal effect strength, in this case, ranges between −0.2 to 0.7. Nevertheless, in more than 79% of the ecoregions, the causal effects between NF and snow depth surpass the significance threshold.

The causality test provides valuable insights into the climatic variable impact (air temperature, snow depth, or both) on NF within each ecoregion, serving as a foundation for designing the copula structure. These values indicate relative statistical influence and should not be interpreted as physical units. Although some previous studies addressed the interrelationship between air temperature and NF[77], snow depth and NF[76], and in some rare cases air temperature, snow depth, and NF[33], they mainly focused on the correlation between the mentioned variables without considering the causal effects.

Having the causal relationship between air temperature, snow depth, and NF, the multivariate statistical approach is calibrated over the observed period. This approach also allows for projections of future changes in NF, considering the compound changes in air temperature and snow depth. In our case, we evaluate two possible future projections using 1000 runs of bootstraps of the statistical multivariate copula. (1) First, we consider a "linear extrapolation," in which future air temperature and snow depth changes are assumed to proceed at the same rate as the observed period (1979–2021). These trends are obtained using the Mann-Kendall trend test and Sen's slope estimator. Then, using the expected changes in air temperature and snow depth by the end of the century, the future NF is projected using copula models. (2) Building upon the range of projected changes in climatic variables derived from the linear extrapolation approach, we characterize the impacts of different levels of change in air temperature and snow depth on NF by systematically evaluating a set of scenarios. By systematically considering these scenarios, we gain a deeper understanding of the interrelationship between air temperature, snow depth, and NF, both in historical contexts and in anticipation of future climatic shifts within the ecoregions. We acknowledge that linear extrapolation cannot fully capture the non-linear dynamics of the climate system, specifically at higher latitudes, where polar amplification and strong feedback processes (*e.g.*, snow and ice albedo, permafrost thaw) play important roles. Our approach should therefore be interpreted as a first-order approximation, providing directional insights rather than precise projections. These trend-informed estimates are broadly consistent with CMIP6 and IPCC projections showing continued reductions in frozen-season duration across northern latitudes but should be viewed as complementary, data-driven benchmarks rather than model-based forecasts.

Based on the "linear extrapolation" results, air temperatures are projected to rise by values between approximately 1 °C to 7 °C with an average of ~3 °C by the end of the century (Fig. 3a). Moving from southern to northern ecoregions, the rate of warming intensifies, where northern Canada and Alaska experience the highest annual air temperature increase. Projected snow depth changes range from 0 cm (no change in annual snow depth) to a 6 cm decrease by the year 2100 (Fig. 3b), with varying patterns across different ecoregions. The future change in NF is then projected under the mentioned air temperature warming and thinning snow depth in each ecoregion using the calibrated copula models (Fig. 3c). The future NF is expected to decrease by approximately 2 to more than 75 days, with an average reduction of more than −30 days across the studied ecoregions. It is worth mentioning that this value should be interpreted as an approximate benchmark of potential magnitude, given the simplicity of the linear extrapolation and the omission of non-linear feedback. The greatest declines in NF occur in Alaska, northern Canada, northern Europe, and eastern Russia. The lower NF due to warming air temperatures and thinner snowpacks can impact the timing and length of phenological, hydrological, and agricultural processes[66], influence the accessibility to natural resources[78], and impact the infrastructure stability and maintenance costs[28] over the northern hemisphere. More intensified declines of NF in higher latitudes, e.g., Alaska, northern Canada, and Russia, hold substantial implications, especially concerning its role in the bearing capacity of roads in northern latitudes and the prolonged and intensified release of greenhouse gas emissions due to permafrost degradation[79,80].

To better understand the climate control on NF, we consider additional scenarios of individual and compound changes in air temperature and snow depth. We evaluate the impacts on NF by combining incremental changes in air temperature (0 °C to +6 °C, sampled every 2 °C), and thinning snow depth (-6 cm to 0 cm, sampled every 2 cm). This configuration results in 25 combinations of scenarios, under which NF is projected under different levels of change in each variable. We complement these scenario surfaces with a trend-informed extrapolation to the end of the 21st century, which provides a first-order benchmark not included in earlier studies. Figure 4 presents the results of this analysis. The dots within each boxplot display the results for specific ecoregions, while larger circles represent the mean for each boxplot. The lines between the boxplots connect the mean values. The boxplots in the Fig. 4a panels show the response of NF to known air temperature changes while the snow depth is shifting from 0 cm to -6 cm. The results for known snow depth changes under increasing air temperatures of 0 °C to +6 °C are displayed in Fig. 4c. Figure 4b, d show the lines connecting

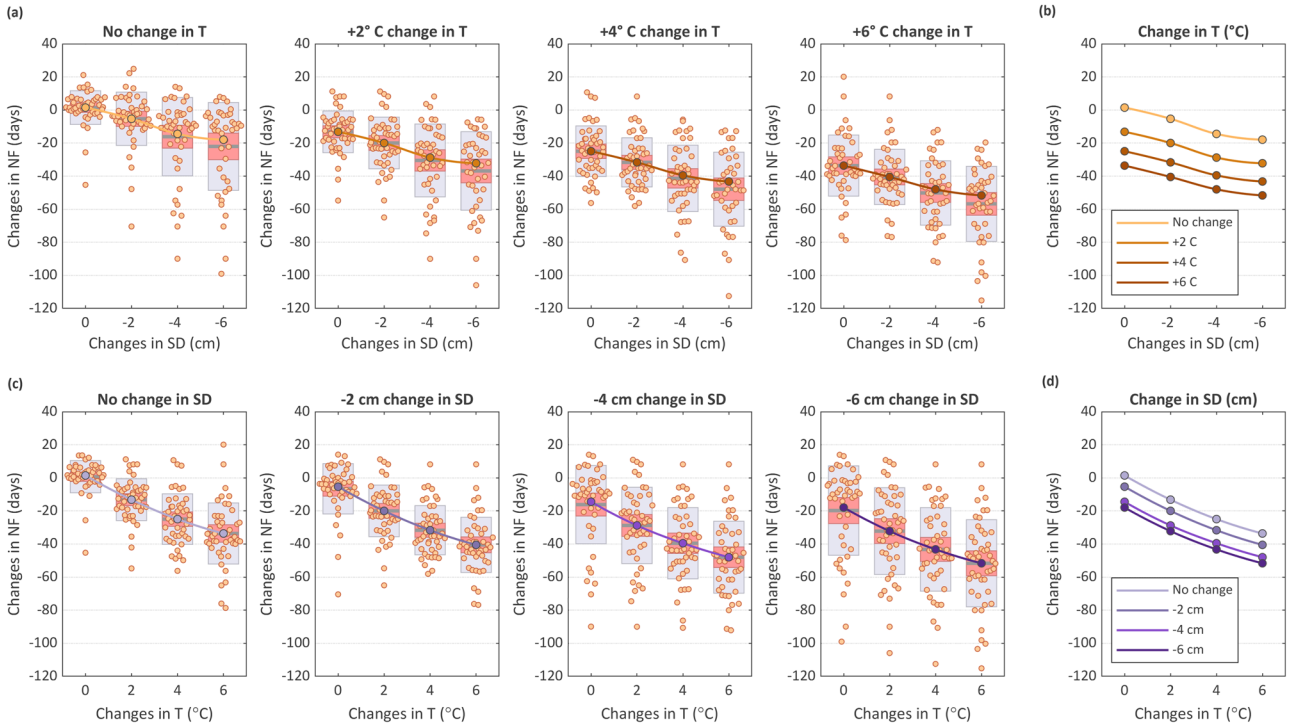

Fig. 4 | Scenario-based analysis of the response of the number of frozen days (NF) to changes in air temperature and snow depth. a and **c** show the NF response under constant air temperature (0 to +6 °C) and constant snow depth (−6 to 0 cm) conditions, respectively. **b** and **d** display the corresponding average NF values for each scenario. Red lines and shading represent NF responses under warming air temperature conditions, while purple lines and shading represent responses under thinning snow depth conditions. The slopes of the lines indicate the relative sensitivity of NF to air temperature and snow depth changes across ecoregions. Box plots show the distribution of NF responses, where the pink shaded band spans the interquartile range and the gray shaded band shows the ±1 standard deviation (SD).

the mean values of boxplots under each scenario. The slope of formed lines provides insight into the relative impacts of air temperature and snow depth on NF.

Looking at the expected change in NF under constant air temperature conditions (Fig. 4a), the wider interquartile ranges under thinner snow depth conditions show higher variability in NF response to increasing snow depth reduction across different ecoregions. For instance, in the first panel of Fig. 4a, under the scenarios of no change in air temperature, different ecoregions experience a range of 32 days (the width of the interquartile range) under 2 cm thinner snow depth. However, the width of the interquartile range increases to more than 50 days under a 6 cm decline in snow depth. Such increases in NF variability under thinner snow conditions suggest that a uniform decrease in snow depth can have very different impacts across regions. This is because snow influences the surface energy budget in multiple, location-dependent ways. For instance, in lower-latitude ecoregions where winter sunlight is relatively strong, a thinner snowpack reduces surface albedo and allows more solar energy to be absorbed by the ground, leading to greater surface warming and thus a larger change in NF. In higher-latitude or colder ecoregions, however, snow's primary role is as an insulator that limits heat loss from the ground during winter[51]. Considering constant snow depth conditions (Fig. 4c), on the other hand, the width of the interquartile range is almost the same under different levels of warming temperature, with less than seven days of difference in most cases. Finally, we compare the slope of the lines for constant air temperature conditions (Fig. 4b; lines in different shades of red) and constant snow depth conditions (Fig. 4d; lines in different shades of purple). The steeper slope of constant snow depth conditions scenarios (average of ~-6 days/°C) compared to the gentler slope for constant air temperature conditions (average of ~−3 days/cm) highlights higher sensitivity of NF to warming temperature, compared to changes in the snow depth. It is worth noting, however, that snow depth is closely linked to temperature and should be understood as a modifying factor that mediates the influence of warming on NF. This interpretation is supported by our causal discovery results, which identify temperature as the dominant driver (T → NF) and snow depth primarily as a conditional mediator (T → SD → NF), while still allowing for pronounced regional effects. Therefore, while our results show that NF is generally more sensitive to air temperature increases than to snow depth changes, it is important to recognize that changes in snow depth can still have pronounced local effects on NF due to the varying energy-budget interactions of snow in different climates. This framing aligns with broader cryosphere feedback processes. Just as temperature-induced declines in northern latitude sea ice or snow cover amplify warming through reduced albedo and altered heat exchange[45,46,81,82], declining snow depth in our study should be viewed as a temperature-driven factor that feeds back onto NF. In other words, temperature initiates changes in both NF and snow depth, and snow depth modulates how strongly these changes manifest in frozen-day counts.

Conclusion and Further Remarks

Climate change can significantly impact the annual accumulation of frozen-days, one of the most important characteristics of freeze-thaw processes and a key component of the cryosphere in northern regions. Changes in FT dynamics can impact regional hydrology, phenology, and land-atmospheric interactions and affect socioeconomic activities such as agriculture and design, construction, and operation of infrastructure. A key emerging question is: How are FT processes changing, and to what extent does this environmental indicator respond to a changing climate? Air temperature and snow depth are identified as major climatic controls on FT dynamics. Our investigation centers on changes in the annual count of frozen days (NF) due to its substantial implications for environmental processes and socioeconomic activities. Our study interprets NF strictly as a measure of surface frozen conditions, and we caution against equating it with subsurface soil freeze or permafrost dynamics. We characterize NF vulnerability to changing climate (i.e., due to warming temperature and thinning snow depth) across more than 47 ecoregions covering the higher latitudes of the northern hemisphere. To address this, we apply an integrated causal

discovery and copula framework. Together with the expanded hemispheric scope, this approach provides important insights into both the primary role of temperature and the modifying influence of snow depth on NF across diverse ecoregions.

Although the annual average air temperature fluctuated greatly over the observed period (1979–2021), all ecoregions experienced warming, and in 85% of ecoregions, the increasing air temperature trends are significant. The average annual snow depth also varied considerably in different ecoregions, where the snow depth decreased significantly in more than 85% of the ecoregions. These changes correspond to a general decrease in NF over the observed period. As demonstrated, the studied ecoregions show a declining NF, with 70% significant trends observed throughout 1979–2021. The correspondence between the trends of NF and the compound changes in air temperature and snow depth highlights the necessity of addressing alterations in FT dynamics in response to shifting climatic conditions.

Analyzing the causal relationship between air temperature/snow depth and NF reveals a significant and consistent causal link in almost all ecoregions. The causal-effect strength between the annual air temperature and NF is significant across all ecoregions, with an average of approximately −0.7. Conversely, the causal links between annual snow depth and NF exhibit greater variability across ecoregions, ranging between −0.2 and 0.7. Nevertheless, over 79% of ecoregions demonstrate statistically significant positive causal connections between snow depth and NF. These findings offer valuable insights into the predominant climatic factors (air temperature, snow depth, or both) influencing NF within each ecoregion.

We also projected future NF changes, considering both air temperature and snow depth alterations with two approaches being used. The first approach is based on "linear extrapolation" of historical trends, while the second systematically evaluates scenario-based combinations of changes in air temperature and snow depth, providing insights into the climatic controls on NF across ecoregions. Under the "linear extrapolation" approach, average annual air temperatures are projected to rise substantially by the end of the century, based solely on observed historical trends. The rate of air temperature warming intensifies from southern to northern ecoregions, with northern ecoregions experiencing the highest increase. Using a similar analysis, annual snow depth is anticipated to decrease overall. By using our casual relationships, the projected changes will result in an average NF reduction of about 30 days across ecoregions. The most pronounced declines in NF are expected in Alaska, northern Canada, northern Europe, and eastern Russia. We acknowledge that linear extrapolation cannot capture non-linear dynamics of the Arctic climate system, including polar amplification and snow-albedo feedback. Our projections should therefore be viewed as a first-order statistical benchmark.

The scenario-based analysis of air temperature and snow depth changes shows that air temperature changes have a more pronounced effect on NF compared to changing snow depth. This analysis also showed a higher variability of declines in NF under thinner snow depth conditions, while the NF is more uniformly decreased under warming air temperature scenarios over different ecoregions. The higher sensitivity of NF to warming air temperatures compared to thinner snow depth conditions provides important insights into the FT dynamics in the context of ongoing and future climate shifts. The reality is that as we extrapolate, snow depth may reach a tipping point threshold, where its influence on NF becomes limited. However, it should be noted that the influence of snow depth on NF can vary by location. A given reduction in snow depth may have a larger effect on NF in some ecoregions than in others due to differences in snow's role in the surface energy budget (reflective cooling versus insulating warmth). Thus, while warming temperature is the dominant driver of NF changes overall, local energy-budget considerations mean that snow depth changes remain an important factor in certain regions. In other words, the snow depth influence is best understood as conditional on temperature, through albedo and insulation effects, rather than as an independent forcing. Although surface radiation was not explicitly modeled here, temperature serves as an effective proxy for net radiative and turbulent fluxes influencing surface energy balance, and thus implicitly captures much of the radiative control on NF. It is also important to note that NF dynamics vary with latitude. As latitude increases, the prevalence of permafrost, ground ice, and cryosphere feedbacks becomes more pronounced, amplifying or modifying NF responses compared to lower-latitude boreal regions.

The proposed methodology enables assessment of compound effects arising from changes in various environmental variables across different spatial and temporal scales at a global extent. However, it is crucial to recognize the potential sensitivity of our findings to data availability and quality, encompassing freeze-thaw and hydroclimatic data, and necessitating a rigorous examination of relative accuracy and uncertainty. This is particularly true when focusing on local impacts. Moreover, when interpreting the results, considering the uncertainty of ERA5 snow-related datasets, such as snow depth, in mountainous regions is of great importance[74,83]. Consequently, to mitigate the diminished accuracy of ERA5 and accurately capture the local climate processes governing FT dynamics in mountainous regions with complex terrain, additional analysis at the regional scale is imperative, utilizing reliable, high-resolution data[84]. It is also important to note that while we focused on snow depth as a large-scale, tractable metric, other snow properties, such as albedo and density, exert strong control over both thermal reflectivity and insulative capacity. These additional characteristics may explain part of the variability we observe across ecoregions and should be considered in future investigations. Future studies could also complement our findings by examining other commonly used snow metrics, such as annual maximum snow depth or snow-cover duration, to provide additional perspectives on snowpack changes. Similarly, while NF provides a simple and tractable proxy for large-scale freeze–thaw dynamics, it does not capture the timing and intensity of individual events. NF should therefore be viewed as a complementary metric that offers a consistent global perspective on frozen conditions, which can be enriched in future studies by integrating event-level measures such as freeze–thaw frequency, soil freeze depth, or transition timing. Finally, we encourage researchers to include the probable impacts of physical characteristics, such as vegetation type, soil type, elevation, and slope, to investigate climate control on FT processes. Beyond its generic utility and a global view, our methodology highlights the asymmetry, nonlinearity, and spatial variability of FT dynamics responses to changing climate conditions on a global scale. Understanding landscape responses to changing freeze and thaw cycles holds important implications, from the risk posed to aging community infrastructures to the regional potential for agriculture and natural resource development to the profound environmental consequences stemming from accelerated permafrost degradation and associated carbon emissions. Addressing these challenges requires integrated and inclusive approaches underpinned by reliable observations and sound scientific knowledge. Building on this foundation, future work could benefit from integrating more sophisticated Earth System model projections (e.g., CMIP6) of air temperature and snow depth into our multivariate copula and causal discovery framework, allowing non-linear cryosphere feedback to be captured more realistically. This would enhance the robustness and policy relevance of our findings and enable direct, high-confidence comparisons with widely used IPCC-compliant climate scenarios. Such integration would also facilitate direct comparison with IPCC-based projections, reinforcing the complementary nature of our empirical approach.

Data

The study area encompasses a total of 47 ecoregions across the higher latitudes (≥45° N) of the northern hemisphere[85]. These ecoregions were selected based on the Terrestrial Ecoregions of the World (TEOW) classification system, which categorizes regions with distinct climate, vegetation, and ecological characteristics[85]. This classification provides a consistent framework for studying climatic and environmental processes across diverse landscapes. The chosen ecoregions represent a wide range of climatic and environmental conditions, from boreal forests to tundra and permafrost zones, ensuring a comprehensive assessment of FT cycle variations. To maintain focus on terrestrial freeze–thaw dynamics, grid cells corresponding to open water, glaciers, or sea-ice regions were masked, as their physical

processes differ fundamentally from land surfaces and are not directly comparable to NF metrics. We extracted monthly air temperature and snow depth data from ERA5 from 1979 to 2021. The ERA5 reanalysis has a 0.25° × 0.25° grid resolution and shows superior performance in accurately replicating observed station data when compared to other global reanalysis products[74,86]. The ERA5 monthly air temperature and snow depth data were then aggregated to obtain yearly (September – August) values over the study period.

We also used the long-term satellite observational record of FT derived from the FT-ESDR[54]. The global FT-ESDR is derived from satellite microwave radiometric brightness temperature (TB) observations that capture the predominant daily freeze or thaw status of the landscape from local morning (AM) and afternoon (PM) satellite overpasses extending from 1979 to 2021 and mapped to a 25 × 25 km² resolution global grid[53]. The FT state is determined using a modified seasonal threshold algorithm, identifying FT transition sequences from the daily brightness temperature (TB) time series. ERA5 surface air temperature records are then used to calibrate the TB threshold between frozen and thawed conditions in the modified seasonal threshold algorithm. The FT-ESDR distinguishes up to four daily FT categories, including frozen (both AM and PM), non-frozen (both AM and PM), transitional (AM frozen and PM thawed), and inverse transitional (AM thawed and PM frozen) states. The FT-ESDR is primarily sensitive to land surface FT conditions as defined from moderate frequency (~37 GHz) TB observations, but is also an indirect indicator of FT in vegetation, snow, and soil layers[87,88]. It reflects the dielectric properties of the surface layer (snow, vegetation, and near-surface soil) as detected by microwave radiometry, indicating whether liquid water is frozen or thawed. Importantly, the FT-ESDR does not directly measure deeper soil freeze or permafrost conditions but rather provides an integrated indicator of surface state. Accordingly, NF derived from FT-ESDR should be interpreted as a measure of surface frozen conditions, not of soil-freeze depth or permafrost state. To ensure consistency between datasets, the ERA5 and FT-ESDR products were brought to a common spatial grid using a *k*-nearest neighbor interpolation scheme, which estimates values based on distance-weighted averages of surrounding grid points.

Using this dataset, we derive the annual (September – August) count of frozen days (Number of Frozen days; NF hereafter). Within the northern hemisphere domain the period between September and August encompasses a complete winter cycle of frozen conditions bounded by predominantly thawed conditions in summer and transitional FT conditions in spring and fall[77,89]. As demonstrated by previous research, NF has important implications for environmental processes and civil infrastructure[90,91]. For example, changes in NF can profoundly impact vegetation growth duration, directly affecting agricultural activities[92]. Additionally, these changes can contribute to increased greenhouse gas emissions due to permafrost thawing[93]. As the copula methodology is sensitive to the existence of autocorrelation, air temperature, snow depth, and NF data are analyzed to investigate the presence of autocorrelation, and the grids with significant autocorrelation are excluded from our analysis.

Method

To examine potential trends in the annual count of frozen days (NF), air temperature, and snow depth, we use the statistical methods of Mann-Kendall and Sen's Slope estimator. The Mann-Kendall test is employed to assess the significance of trends, while Sen's Slope estimator is utilized to determine the rate of change. The significance of these trends is determined by examining the associated *p*-value, which is set at a threshold of 0.05 in this study. Moreover, we employ a causal discovery approach[94–96] to investigate the influence of air temperature and snow depth on NF in different ecoregions across the higher latitudes of the northern hemisphere (≥45°N). Here, the term 'causal' is used in the statistical sense, referring to directed dependencies inferred from conditional independence tests and temporal ordering, and does not imply direct physical causation. To ensure that causal relationships are not confounded by long-term trends and shared external influences, we linearly detrended all variables prior to assessing causality. This prevents spurious correlations that may arise from common trends rather than direct causal links[94,95,97]. Non-climatic factors can also influence NF, including soil organic matter, solar radiation, and disturbances such as wildfires. In this study, however, we focus exclusively on the climatic controls of NF, as they explain most of its variability.

Specifically, we investigated the causal effects of air temperature and snow depth on NF. In the causal discovery approach, the initial step involves constructing a directed acyclic graph (DAG) to reveal the causal relationships among the variables under consideration. This graphical representation elucidates the causal structure of the system, with nodes representing variables and directed edges denoting causal connections. PCMCI+ has been increasingly applied in hydrology and climatology for causal inference, particularly in disentangling complex dependencies in climate and environmental systems[94,98–100]. We employ the PCMCI+ algorithm for DAG construction[97]. This algorithm begins with a fully connected graph and iteratively assesses the removal of links between variables, considering expanding sets of conditions (Supplementary Fig. 1). The PCMCI+ algorithm outperforms traditional correlation analysis by identifying linkages that correlations may miss[101]. Moreover, it is particularly effective at accounting for common drivers and detecting indirect links, setting it apart from other causal discovery approaches such as Granger causality[95].

In practical terms, PCMCI+ first identifies potential links based on conditional independence tests and then quantifies their statistical strength. "Causal strength" here refers to a normalized, dimensionless test statistic (ranging from 0 to ±1) that reflects the relative influence of one variable on another in the time series, rather than a physical rate or mechanistic cause. To distinguish direct and indirect influences among variables, PCMCI+ tests conditional independencies across time lags to recover directed dependencies among air temperature, snow depth, and NF. This enables us to identify both direct (e.g., T → NF) and mediated effects (e.g., T → SD → NF), while ensuring that snow depth is modeled conditional on temperature. In this way, snow depth is represented as a modifying factor rather than an entirely independent driver, though the algorithm still detects significant causal contributions where present.

The causal discovery algorithm comprises two key stages. First, it employs the PC1, a Markov set discovery algorithm derived from the PC-stable algorithm[102], to eliminate irrelevant conditions for each variable through an iterative process of independence testing. In this phase, linear partial correlation is employed for conditional independence testing, with a significance level of 0.05, ensuring that only relevant conditions are retained in the analysis. In the second stage, the momentary conditional independence (MCI) test leverages the conditions identified in the previous step to infer the causal connections. While the primary goal of the PCMCI+ algorithm is to identify the causal graph, the MCI test statistics also provide a precise measure of normalized causal strength (CMI, conditional mutual information), ranging from 0 (weakest) to ±1 (strongest. This facilitates the interpretation of the identified links. This measure enables the assessment of the strength of causal relationships among variables[103]. A Python software tool is used to estimate the causal network to execute this process; it is provided at: https://tocsy.pik-potsdam.de/tigramite.php.

We describe the joint dependencies between detrended NF (NF_t), air temperature (T_t), and snow depth (SD_t) using multivariate copulas. According to Sklar's theorem, if we denote the marginal cumulative distribution functions (CDFs) of NF, air temperature (T), and snow depth (SD) as $F_1(NF_t)$, $F_2(T_t)$, and $F_3(SD_t)$, respectively, then we can express the joint dependency structure, $F(NF_t, T_t, SD_t)$, using the trivariate copula function (C), as follows[104]:

$$F(NF_t, T_t, SD_t) = C(F_1(NF_t), F_2(T_t), F_3(SD_t)) \quad (1)$$

Based on empirical characteristics, several potential probability distributions are assessed to determine the most appropriate parametric distribution, considering the Bayesian Information Criterion. We employ a canonical vine (C-vine) copula to construct the probabilistic model. This d-dimensional C-vine structure combines bivariate copula pairs arranged

into (d-1) trees, allowing for the possibility that each bivariate pair may belong to distinct parametric families.

Using the C-vine copula, the joint distribution between the studied variables can be described as:

$$f(\mathrm{NF}_t, T_t, \mathrm{SD}_t) = f_2(T_t) f_{3|2}(\mathrm{SD}_t|T_t) f_{1|2,3}(NF_t|T_t, \mathrm{SD}_t) \quad (2)$$

where the marginal PDFs are shown by $f(.)$. The conditional distributions can be estimated as[105]:

$$f_{3|2}(\mathrm{SD}_t|T_t) = \frac{f(\mathrm{SD}_t, T_t)}{f(T_t)} = \frac{c_{2,3}(F_2(T_t), F_3(\mathrm{SD}_t)) f_2(T_t) f_3(\mathrm{SD}_t)}{f_2(T_t)} = c_{2,3}(F_2(T_t), F_3(\mathrm{SD}_t)) f_3(\mathrm{SD}_t) \quad (3)$$

and

$$f_{1|2,3}(NF_t|T_t, SD_t) = \frac{f(NF_t, SD_t|T_t)}{f(SD_t|T_t)} = \frac{c_{1,3|2}(F(NF_t|T_t), F(\mathrm{SD}_t|T_t)) f(NF_t|T_t) f(\mathrm{SD}_t|T_t)}{f(SD_t|T_t)} = c_{1,3|2}(F(NF_t|T_t), F(SD_t|T_t)) c_{1,2}(F_1(NF_t), F_2(T_t)) f_1(NF_t) \quad (4)$$

where $c(\cdot)$ is the 3-dimensional copula density[106]. As a result, the three-dimensional joint density can be represented in terms of bivariate copulas as follows:

$$f(NF_t, T_t, \mathrm{SD}_t) = f_1(NF_t).f_2(T_t).f_3(\mathrm{SD}_t).c_{2,1}.c_{2,3}.c_{1,3|2} \quad (5)$$

where $c_{2,1}$, $c_{2,3}$ and $c_{1,3|2}$ are the densities of bivariate pairs. $c_{2,1}$ and $c_{2,3}$ are $c_{2,1}(F_2(T_t), F_1(NF_t))$ and $c_{2,3}(F_2(T_t), F_3(SD_t))$. $c_{1,3|2}$ are the conditional pairwise copulas between $F_1(NF_t)$ and $F_3(SD_t)$ conditional to $F_2(T_t)$, i.e., $c_{1,3|2}(F_1(NF_t), F_3(SD_t)|F_2(T_t))$. Importantly, this structure explicitly considers the conditional dependence of snow depth on temperature, through the term $f_{3|2}(\mathrm{SD}_t|T_t)$. In other words, snow depth is not treated as fully independent of temperature, but rather as a modifying factor whose probability distribution is conditioned on temperature when modeling its influence on NF. The analysis is conducted in CRAN R with packages VineCopula, CDVine, and copula[107–109].

To quantitively measure the interdependence between NF, T, and SD, we use Kendall's τ dependence coefficient. Kendall's τ is a non-parametric dependence test with the empirical formulation:

$$\tau_{X,Y} = \frac{n_c - n_d}{\binom{n}{2}} \quad (6)$$

where n_c and n_d are the number of concordant and discordant pairs, respectively and X and Y are the pair of random variables[110]. The significance of the dependence is evaluated by a formal p-value associated with Kendall's τ dependence coefficient. In this study, p-value = 0.05 is considered as the threshold of meaningful dependence.

We evaluated the performance of the copula methodology in capturing the observed interdependencies between involved variables, *i.e.*, NF, air temperature, and snow depth. For this purpose, we first identify the interdependencies between NF and air temperature ($\tau_{NF,T}$), and NF and snow depth ($\tau_{NF,SD}$) using the observed values and then evaluate the effectiveness of our multivariate model in capturing these observed interconnections. We randomly generate 1000 sets of variables of the same size as the observed data in each ecoregion. Subsequently, we calculate the value of Kendall's τ, which quantifies dependence, using the simulated pairs. The simulated range is then compared with the observed values, enabling us to gauge the copula model's efficacy in accurately representing the observed dependencies – see Supplementary Fig. 2. The boxplots show the range of simulated dependencies $\tau_{NF,T}$ (Supplementary Fig. 2a) and $\tau_{NF,SD}$ (Supplementary Fig. 2b), while the blue and red dots show the observed values. Considering the interrelationships among hydroclimatic variables and NF at an annual scale, we observe an average relative error of less than 7% when representing Kendall's τ for all ecoregions.

We also validate the performance of the copula methodology in capturing the time series of NF by comparing the simulated NF generated by the copula models drawing on air temperature and snow depth data from ERA5 to the observed NF values obtained from the FT-ESDR over the testing phase (2001–2010) – see Supplementary Fig. 3. For this purpose, we show the range of errors in 1000 sets of simulated NF across each of the 47 ecoregions studied over the northern hemisphere (Supplementary Fig. 3a). In Supplementary Fig. 3b, we further show the mean error in simulated NF in the testing phase across the studied ecoregions. Based on the observations, the error in simulated NF over the observed period is less than 5 days in more than 75% of the considered ecoregions.

Data availability

The datasets used and analyzed in this study are derived from publicly available sources. The FT data is obtained from the Global Freeze/Thaw Earth System Data Record (FT-ESDR), accessible via the National Snow and Ice Data Center (NSIDC) (https://nsidc.org/data/nsidc-0477/versions/5). The meteorological variables, including air temperature and snow depth, are sourced from the ERA5 reanalysis dataset provided by the European Centre for Medium-Range Weather Forecasts (ECMWF) (https://doi.org/10.24381/cds.f17050d7). Simulated NF data in this study is available at https://doi.org/10.17605/OSF.IO/97CVX.

Code availability

No custom code was developed for this study. The causal network analysis was performed using the Python-based Tigramite package (https://tocsy.pik-potsdam.de/tigramite.php). Additional statistical analyses were carried out in MATLAB (R2023a) and CRAN R using standard packages, including *VineCopula*, *CDVine*, and *copula*[107–109].

Received: 27 May 2025; Accepted: 20 November 2025;
Published online: 08 December 2025

References

1. Derksen, C. et al. Retrieving landscape freeze/thaw state from Soil Moisture Active Passive (SMAP) radar and radiometer measurements. *Remote Sens. Environ.* **194**, 48–62 (2017).
2. Vonk, J. E., Tank, S. E. & Walvoord, M. A. Integrating hydrology and biogeochemistry across frozen landscapes. *Nat. Commun.* **10**, 5377 (2019).
3. Plaza, C. et al. Direct observation of permafrost degradation and rapid soil carbon loss in tundra. *Nat. Geosci.* **12**, 627–631 (2019).
4. Xie, S., Jian-jun, Q., Yuan-ming, L., Zhi-wei, Z. & Xiang-tian, X. Effects of freeze-thaw cycles on soil mechanical and physical properties in the Qinghai-Tibet Plateau. *J. Mt. Sci.* **12**, 999–1009 (2015).
5. Hopping, K. A., Chignell, S. M. & Lambin, E. F. The demise of caterpillar fungus in the Himalayan region due to climate change and overharvesting. *Proc. Natl. Acad. Sci.* **115**, 11489–11494 (2018).
6. Wang, R., Hu, Z., Li, Y., Wang, K. & Zhang, H. Review on the deterioration and approaches to enhance the durability of concrete in the freeze–thaw environment. *Constr. Build. Mater.* **321**, 126371 (2022).
7. Liu, J., Chang, D. & Yu, Q. Influence of freeze-thaw cycles on mechanical properties of a silty sand. *Eng. Geol.* **210**, 23–32 (2016).
8. Wang, K., Zhang, T. & Zhong, X. Changes in the timing and duration of the near-surface soil freeze/thaw status from 1956 to 2006 across China. *Cryosphere* **9**, 1321–1331 (2015).
9. Zhang, X. et al. Effects of changes in Freeze-Thaw cycles on soil hydrothermal dynamics and erosion degradation under global warming in the Black Soil Region. *Water Resour. Res.* **61**, e2024WR038318 (2025).

10. Ge, Z., Li, G., Dun, H. & Huang, N. Freeze-thaw characteristics and deformation monitoring of topsoil in highland pastoral areas under the influence of snow accumulation. *Heliyon* **10**, e33652 (2024).
11. Arenson, L. U., Kääb, A. & O'Sullivan, A. Detection and analysis of ground deformation in permafrost environments. *Permafr. Periglac. Process.* **27**, 339–351 (2016).
12. Bechmann, M. E., Kleinman, P. J. A., Sharpley, A. N. & Saporito, L. S. Freeze–Thaw Effects on Phosphorus Loss in Runoff from Manured and Catch-Cropped Soils. *J. Environ. Qual.* **34**, 2301–2309 (2005).
13. Colombo, N. et al. Review: Impacts of permafrost degradation on inorganic chemistry of surface fresh water. *Glob. Planet. Change* **162**, 69–83 (2018).
14. Li, J. et al. Weakening warming on spring freeze–thaw cycle caused greening Earth's third pole. *Proc. Natl. Acad. Sci.* **121**, e2319581121 (2024).
15. Fasaeiyan, N., Jung, S., Boudreault, R., Arenson, L. U. & Maghoul, P. A review on mathematical modeling of microbial and plant induced permafrost carbon feedback. *Sci. Total Environ.* **939**, 173144 (2024).
16. Natali, S. M. et al. Large loss of CO2 in winter observed across the northern permafrost region. *Nat. Clim. Chang.* **9**, 852–857 (2019).
17. Teufel, B. & Sushama, L. Abrupt changes across the Arctic permafrost region endanger northern development. *Nat. Clim. Chang.* **9**, 858–862 (2019).
18. Wang, J., Luo, S., Li, Z., Wang, S. & Li, Z. The freeze/thaw process and the surface energy budget of the seasonally frozen ground in the source region of the Yellow River. *Theor. Appl Climatol.* **138**, 1631–1646 (2019).
19. Rooney, E. C. et al. The Impact of Freeze-Thaw History on Soil Carbon Response to Experimental Freeze-Thaw Cycles. *J. Geophys. Res.: Biogeosci.* **127**, e2022JG006889 (2022).
20. Wagner-Riddle, C. et al. Globally important nitrous oxide emissions from croplands induced by freeze–thaw cycles. *Nat. Geosci.* **10**, 279–283 (2017).
21. Congreves, K. A., Wagner-Riddle, C., Si, B. C. & Clough, T. J. Nitrous oxide emissions and biogeochemical responses to soil freezing-thawing and drying-wetting. *Soil Biol. Biochem.* **117**, 5–15 (2018).
22. Hu, G. et al. Thermal properties of active layer in permafrost regions with different vegetation types on the Qinghai-Tibetan Plateau. *Theor. Appl Climatol.* **139**, 983–993 (2020).
23. Parry M. L. *Climate Change and World Agriculture* (Routledge, 2019).
24. O'Neill, H. B. et al. Permafrost thaw and northern development. *Nat. Clim. Chang.* **10**, 722–723 (2020).
25. Rooney, E. C. & Possinger, A. R. Climate and Ecosystem Factors Mediate Soil Freeze-Thaw Cycles at the Continental Scale. *J. Geophys Res Biogeosci.* **129**, e2024JG008009 (2024).
26. Polyakov I. V. et al. Observationally based assessment of polar amplification of global warming. *Geophys. Res. Lett.* **29**, 25-1-25–4 (2002).
27. Liu, Z. et al. Widespread deepening of the active layer in northern permafrost regions from 2003 to 2020. *Environ. Res. Lett.* **19**, 014020 (2023).
28. Park, H., Kim, Y. & Kimball, J. S. Widespread permafrost vulnerability and soil active layer increases over the high northern latitudes inferred from satellite remote sensing and process model assessments. *Remote Sens. Environ.* **175**, 349–358 (2016).
29. Magnússon, R. Í et al. Extremely wet summer events enhance permafrost thaw for multiple years in Siberian tundra. *Nat. Commun.* **13**, 1556 (2022).
30. Gibson, C. M. et al. Wildfire as a major driver of recent permafrost thaw in boreal peatlands. *Nat. Commun.* **9**, 3041 (2018).
31. Guo, W. et al. Vegetation can strongly regulate permafrost degradation at its southern edge through changing surface freeze-thaw processes. *Agric. For. Meteorol.* **252**, 10–17 (2018).
32. Walz, J., Knoblauch, C., Böhme, L. & Pfeiffer, E.-M. Regulation of soil organic matter decomposition in permafrost-affected Siberian tundra soils - Impact of oxygen availability, freezing and thawing, temperature, and labile organic matter. *Soil Biol. Biochem.* **110**, 34–43 (2017).
33. Hatami, S. & Nazemi, A. Compound changes in temperature and snow depth lead to asymmetric and nonlinear responses in landscape freeze–thaw. *Sci. Rep.* **12**, 2196 (2022).
34. Henry, H. A. L. Climate change and soil freezing dynamics: historical trends and projected changes. *Clim. Change* **87**, 421–434 (2008).
35. Wipf, S., Sommerkorn, M., Stutter, M. I., Wubs, E. R. J. & van der Wal, R. Snow cover, freeze-thaw, and the retention of nutrients in an oceanic mountain ecosystem. *Ecosphere* **6**, art207 (2015).
36. Mena, G. et al. Freeze–thaw cycles and snow impact at arid permafrost region in Chajnantor Volcano, Atacama, northern Chile. *Arct., Antarct., Alp. Res.* **53**, 60–66 (2021).
37. Hollesen, J., Matthiesen, H., Møller, A. B. & Elberling, B. Permafrost thawing in organic Arctic soils accelerated by ground heat production. *Nat. Clim. Change* **5**, 574–578 (2015).
38. Kim, Y. et al. Attribution of divergent northern vegetation growth responses to lengthening non-frozen seasons using satellite optical-NIR and microwave remote sensing. *Int. J. Remote Sens.* **35**, 3700–3721 (2014).
39. Sinha, T. & Cherkauer, K. A. Time Series Analysis of Soil Freeze and Thaw Processes in Indiana. *J. Hydrometeorol.* **9**, 936–950 (2008).
40. Chen, L. et al. Influences of forest cover on soil freeze-thaw dynamics and greenhouse gas emissions through the regulation of snow regimes: A comparison study of the farmland and forest plantation. *Sci. Total Environ.* **726**, 138403 (2020).
41. Hirota, T. et al. Soil frost control: agricultural adaptation to climate variability in a cold region of Japan. *Mitig. Adapt Strateg Glob. Change* **16**, 791–802 (2011).
42. Fletcher C. G., Kushner P. J., Hall A., Qu X., Circulation responses to snow albedo feedback in climate change. *Geophysical Research Letters* **36** (2009).
43. Kim, Y., Kimball, J. S., Du, J., Schaaf, C. L. B. & Kirchner, P. B. Quantifying the effects of freeze-thaw transitions and snowpack melt on land surface albedo and energy exchange over Alaska and Western Canada. *Environ. Res. Lett.* **13**, 075009 (2018).
44. Kattsov, V. M. et al. Simulation and Projection of Arctic Freshwater Budget Components by the IPCC AR4 Global Climate Models. *J. Hydrometeorol.* **8**, 571–589 (2007).
45. Cohen, J. et al. Recent Arctic amplification and extreme mid-latitude weather. *Nat. Geosci.* **7**, 627–637 (2014).
46. Flanner, M. G., Shell, K. M., Barlage, M., Perovich, D. K. & Tschudi, M. A. Radiative forcing and albedo feedback from the Northern Hemisphere cryosphere between 1979 and 2008. *Nat. Geosci.* **4**, 151–155 (2011).
47. Ding, S., Zou, Y. & Yu, X. Freeze-thaw cycles alter the growth sprouting strategy of wetland plants by promoting denitrification. *Commun. Earth Environ.* **4**, 1–11 (2023).
48. Pi, K. et al. The Cold Region Critical Zone in Transition: Responses to Climate Warming and Land Use Change. *Annu. Rev. Environ. Resour.* **46**, 111–134 (2021).
49. Chmura, H. E. et al. Climate change is altering the physiology and phenology of an arctic hibernator. *Science* **380**, 846–849 (2023).
50. Iwata Y., Hayashi M., Suzuki S., Hirota T. & Hasegawa S. Effects of snow cover on soil freezing, water movement, and snowmelt infiltration: A paired plot experiment. *Water Resources Res.* **46** (2010).
51. Zhang T. Influence of the seasonal snow cover on the ground thermal regime: An overview. *Rev. Geophys.* **43** (2005).
52. Shati, F., Prakash, S., Norouzi, H. & Blake, R. Assessment of differences between near-surface air and soil temperatures for reliable detection of high-latitude freeze and thaw states. *Cold Reg. Sci. Technol.* **145**, 86–92 (2018).

53. Kim, Y., Kimball, J. S., McDonald, K. C. & Glassy, J. Developing a Global Data Record of Daily Landscape Freeze/Thaw Status Using Satellite Passive Microwave Remote Sensing. *IEEE Trans. Geosci. Remote Sens.* **49**, 949–960 (2011).
54. Kim Y., Kimball J., Du J. & Glassy J. MEaSUREs Global Record of Daily Landscape Freeze/Thaw Status, Version 5. *NASA National Snow and Ice Data Center Distributed Active Archive Center (DAAC) data set* LJ6SLXNJB2CQ. https://doi.org/10.5067/LJ6SLXNJB2CQ (2021).
55. Meshesha, T. W., Wang, J. & Melaku, N. D. Modelling spatiotemporal patterns of water quality and its impacts on aquatic ecosystem in the cold climate region of Alberta, Canada. *J. Hydrol.* **587**, 124952 (2020).
56. Williams, C. M., Henry, H. A. L. & Sinclair, B. J. Cold truths: how winter drives responses of terrestrial organisms to climate change. *Biol. Rev.* **90**, 214–235 (2015).
57. Schaefer, K., Lantuit, H., Romanovsky, V. E., Schuur, E. A. G. & Witt, R. The impact of the permafrost carbon feedback on global climate. *Environ. Res. Lett.* **9**, 085003 (2014).
58. Wu, Y. et al. Assessment of soil erosion characteristics in response to temperature and precipitation in a freeze-thaw watershed. *Geoderma* **328**, 56–65 (2018).
59. Melvin, A. M. et al. Climate change damages to Alaska public infrastructure and the economics of proactive adaptation. *Proc. Natl. Acad. Sci.* **114**, E122–E131 (2017).
60. Zwissler, B., Oommen, T. & Vitton, S. A Study of the Impacts of Freeze–Thaw on Cliff Recession at the Calvert Cliffs in Calvert County, Maryland. *Geotech. Geol. Eng.* **32**, 1133–1148 (2014).
61. Qiao, Y. et al. Contrasting sensitivity of air temperature trends to surface soil temperature trends between climate models and reanalyses. *npj Clim. Atmos. Sci.* **7**, 1–11 (2024).
62. Hersbach, H. et al. The ERA5 global reanalysis. *Q. J. R. Meteorol. Soc.* **146**, 1999–2049 (2020).
63. Kim Y., Kimball J. S., Du J. & Glassy J. A Global Data Record of Daily Landscape Freeze/Thaw status Version 5. https://doi.org/10.5067/LJ6SLXNJB2CQ. Deposited 1 January 2023.
64. Schuur, E. A. G. et al. Climate change and the permafrost carbon feedback. *Nature* **520**, 171–179 (2015).
65. Carpino, O. A., Berg, A. A., Quinton, W. L. & Adams, J. R. Climate change and permafrost thaw-induced boreal forest loss in northwestern Canada. *Environ. Res. Lett.* **13**, 084018 (2018).
66. Sharma, S., Szele, Z., Schilling, R., Munch, J. C. & Schloter, M. Influence of Freeze-Thaw Stress on the Structure and Function of Microbial Communities and Denitrifying Populations in Soil. *Appl. Environ. Microbiol.* **72**, 2148–2154 (2006).
67. Gaupp, F., Hall, J., Hochrainer-Stigler, S. & Dadson, S. Changing risks of simultaneous global breadbasket failure. *Nat. Clim. Chang.* **10**, 54–57 (2020).
68. Zaerpour, M., Papalexiou, S. M. & Nazemi, A. Informing Stochastic Streamflow Generation by Large-Scale Climate Indices at Single and Multiple Sites. *Adv. Water Resour.* **156**, 104037 (2021).
69. Zhou, S. et al. Land–atmosphere feedbacks exacerbate concurrent soil drought and atmospheric aridity. *Proc. Natl. Acad. Sci.* **116**, 18848–18853 (2019).
70. Rosenzweig, C. et al. Attributing physical and biological impacts to anthropogenic climate change. *Nature* **453**, 353–357 (2008).
71. Wieder, W. R. et al. Pervasive alterations to snow-dominated ecosystem functions under climate change. *Proc. Natl. Acad. Sci.* **119**, e2202393119 (2022).
72. Hatami S. & Nazemi A. The Compound Impacts of Changing Temperature and Snow Cover on Freeze and Thaw Patterns across Québec. *Geo-Extreme Ascelibrary* 368–376. https://doi.org/10.1061/9780784483701.035 (2021).
73. Liston G. E. & Elder K. A Distributed Snow-Evolution Modeling System (SnowModel). https://doi.org/10.1175/JHM548.1 (2006).
74. Mortimer, C. et al. Evaluation of long-term Northern Hemisphere snow water equivalent products. *Cryosphere* **14**, 1579–1594 (2020).
75. Sturm M. et al. Estimating Snow Water Equivalent Using Snow Depth Data and Climate Classes. https://doi.org/10.1175/2010JHM1202.1 (2010).
76. Yi, Y., Kimball, J. S., Rawlins, M. A., Moghaddam, M. & Euskirchen, E. S. The role of snow cover affecting boreal-arctic soil freeze–thaw and carbon dynamics. *Biogeosciences* **12**, 5811–5829 (2015).
77. Hatami, S. & Nazemi, A. A statistical framework for assessing temperature controls on landscape Freeze-Thaw: Application and implications in Québec, Canada (1979–2016). *J. Hydrol.* **603**, 126891 (2021).
78. Poppel B., Siegstad M., Fægteborg M. & Snyder H. The Arctic as a 'hotspot' for natural resource extraction and global warming In, pp. 129–135. (2017)
79. Kraatz, S., Jacobs, J. M. & Miller, H. J. Spatial and temporal freeze-thaw variations in Alaskan roads. *Cold Reg. Sci. Technol.* **157**, 149–162 (2019).
80. Kraatz, S., Miller, H. J. & Jacobs, J. M. Remotely Sensed Freeze-Thaw from the Soil Moisture Active Passive Instrument to Inform the Timing of Seasonal Load Restrictions in Alaska. *Transp. Res. Rec.* **2673**, 410–418 (2019).
81. Serreze, M. C. & Barry, R. G. Processes and impacts of Arctic amplification: A research synthesis. *Glob. Planet. Change* **77**, 85–96 (2011).
82. Screen, J. A. & Simmonds, I. The central role of diminishing sea ice in recent Arctic temperature amplification. *Nature* **464**, 1334–1337 (2010).
83. Lei, Y., Pan, J., Xiong, C., Jiang, L. & Shi, J. Snow depth and snow cover over the Tibetan Plateau observed from space in against ERA5: matters of scale. *Clim. Dyn.* **60**, 1523–1541 (2023).
84. Cho, E., McCrary, R. R. & Jacobs, J. M. Future Changes in Snowpack, Snowmelt, and Runoff Potential Extremes Over North America. *Geophys. Res. Lett.* **48**, e2021GL094985 (2021).
85. Olson, D. M. et al. Terrestrial Ecoregions of the World: A New Map of Life on Earth: A new global map of terrestrial ecoregions provides an innovative tool for conserving biodiversity. *BioScience* **51**, 933–938 (2001).
86. Urraca, R. et al. Evaluation of global horizontal irradiance estimates from ERA5 and COSMO-REA6 reanalyses using ground and satellite-based data. *Sol. Energy* **164**, 339–354 (2018).
87. Podest, E., McDonald, K. C. & Kimball, J. S. Multisensor Microwave Sensitivity to Freeze/Thaw Dynamics Across a Complex Boreal Landscape. *IEEE Trans. Geosci. Remote Sens.* **52**, 6818–6828 (2014).
88. Donahue, K. et al. Deep learning estimation of northern hemisphere soil freeze-thaw dynamics using satellite multi-frequency microwave brightness temperature observations. *Front. Big Data* **6**, 1243559 (2023).
89. Kim, Y., Kimball, J. S., Glassy, J. & Du, J. An extended global Earth system data record on daily landscape freeze–thaw status determined from satellite passive microwave remote sensing. *Earth Syst. Sci. Data* **9**, 133–147 (2017).
90. Sorensen, P. O. et al. Winter soil freeze-thaw cycles lead to reductions in soil microbial biomass and activity not compensated for by soil warming. *Soil Biol. Biochem.* **116**, 39–47 (2018).
91. Zhang, P., Wittmann, F. H., Vogel, M., Müller, H. S. & Zhao, T. Influence of freeze-thaw cycles on capillary absorption and chloride penetration into concrete. *Cem. Concr. Res.* **100**, 60–67 (2017).
92. Margesin, R., Neuner, G. & Storey, K. B. Cold-loving microbes, plants, and animals—fundamental and applied aspects. *Naturwissenschaften* **94**, 77–99 (2007).
93. Turetsky, M. R. et al. Carbon release through abrupt permafrost thaw. *Nat. Geosci.* **13**, 138–143 (2020).

94. Runge, J., Nowack, P., Kretschmer, M., Flaxman, S. & Sejdinovic, D. Detecting and quantifying causal associations in large nonlinear time series datasets. *Sci. Adv.* **5**, eaau4996 (2019).
95. Runge, J. et al. Inferring causation from time series in Earth system sciences. *Nat. Commun.* **10**, 2553 (2019).
96. Spirtes P., Glymour C. N., Scheines R., *Causation, Prediction, and Search* (MIT Press, 2000).
97. Runge, J. et al. Identifying causal gateways and mediators in complex spatio-temporal systems. *Nat. Commun.* **6**, 8502 (2015).
98. Zaerpour, M. et al. Climate shapes baseflows, influencing drought severity. *Environ. Res. Lett.* **20**, 014035 (2024).
99. Zaerpour, M. et al. Impacts of agriculture and snow dynamics on catchment water balance in the U.S. and Great Britain. *Commun. Earth Environ.* **5**, 1–14 (2024).
100. Zaerpour, M. et al. Agriculture's impact on water–energy balance varies across climates. *Proc. Natl. Acad. Sci.* **122**, e2410521122 (2025).
101. Almendra-Martín, L. et al. Influence of atmospheric patterns on soil moisture dynamics in Europe. *Sci. Total Environ.* **846**, 157537 (2022).
102. Colombo, D. & Maathuis, M. H. Order-Independent Constraint-Based Causal Structure Learning. *J. Mach. Learn. Res.* **15**, 3921–3962 (2014).
103. Runge, J. Quantifying information transfer and mediation along causal pathways in complex systems. *Phys. Rev. E* **92**, 062829 (2015).
104. Sklar, M. Fonctions de répartition à N dimensions et leurs marges. *Annales de. l'ISUP* **VIII**, 229–231 (1959).
105. Aas, K., Czado, C., Frigessi, A. & Bakken, H. Pair-copula constructions of multiple dependence. *Insurance: Math. Econ.* **44**, 182–198 (2009).
106. Joe H. *Multivariate models and multivariate dependence concepts* (CRC Press, 1997).
107. Brechmann, E. C. & Schepsmeier, U. Modeling Dependence with C- and D-Vine Copulas: The R Package CDVine. *J. Stat. Softw.* **52**, 1–27 (2013).
108. Schepsmeier U. et al. Package 'VineCopula.' (2015).
109. Yan, J. Enjoy the Joy of Copulas: With a Package copula. *J. Stat. Softw.* **21**, 1–21 (2007).
110. Genest, C. & Favre, A.-C. Everything You Always Wanted to Know about Copula Modeling but Were Afraid to Ask. *J. Hydrol. Eng.* **12**, 347–368 (2007).

Acknowledgements

We thank Mitacs Elevate and Iron Ore Company of Canada - Rio Tinto for providing financial support for this study. We want to extend our appreciation to the University of Calgary and McGill University for providing technical support throughout this research. We acknowledge the support of the Natural Sciences and Engineering Research Council of Canada to authors S.H. and S.M.P. through NSERC Discovery Grant (RGPIN-2019-06894). Thanks also go to the Iron Ore Company of Canada and Rio Tinto staff who helped with this work, especially J. Wentzell, A. Magee, and P. Lauziere. We are also grateful to the Associate Editor and the three reviewers for their constructive feedback, which greatly improved the clarity and quality of this manuscript.

Author contributions

S.H. designed the study, conducted the analyses, developed the methodological framework, and prepared the figures. M.Z. and A.S.B. contributed to methodological development, statistical analysis, and interpretation of results. J.F.A., S.M.P., A.P., and J.K. supervised the research, contributed to study design, guided the analysis, and led the interpretation of results. All authors discussed the results and contributed to the final manuscript.

Competing interests

The authors declare no competing interests.

Additional information

Supplementary information The online version contains supplementary material available at https://doi.org/10.1038/s43247-025-03059-6.

Correspondence and requests for materials should be addressed to Masoud Zaerpour.

Peer review information *Communications Earth and Environment* thanks Geoffrey Wilson, Yating Chen, and the other anonymous reviewer(s) for their contribution to the peer review of this work. Primary Handling Editors: Min-Hui Lo and Alice Drinkwater. [A peer review file is available].